Soft Matter

Jamming on convex deformable surfaces

Journal:	*Soft Matter*
Manuscript ID	SM-ART-12-2022-001608.R2
Article Type:	Paper
Date Submitted by the Author:	03-Jan-2024
Complete List of Authors:	Xie, Zhaoyu; Tufts University School of Arts and Sciences, Physics and Astronomy Atherton, Tim; Tufts University, Physics and Astronomy

Soft Matter

ARTICLE TYPE

Cite this: DOI: 00.0000/xxxxxxxxxx

Jamming on convex deformable surfaces†

Zhaoyu Xie,[a] and Timothy J. Atherton[a,b]

Received Date
Accepted Date

DOI: 00.0000/xxxxxxxxxx

Jamming is a fundamental transition that governs the behavior of particulate media, including sand, foams and dense suspensions. Upon compression, such media change from freely flowing to a disordered, marginally stable solid that exhibits non-Hookean elasticity. While the jamming process is well established for fixed geometries, the nature and dynamics of jamming for a diverse class of soft materials and deformable substrates, including emulsions and biological matter, remains unknown. Here we propose a new scenario, metric jamming, where rigidification occurs on a surface that has been deformed from its ground state. Unlike classical jamming processes that exhibit discrete mechanical transitions, surprisingly we find that metric jammed states possess mechanical properties continuously tunable between those of classically jammed and conventional elastic media. The compact and curved geometry significantly alters the vibrational spectra of the structures relative to jamming in flat Euclidean space, and metric jammed systems also possess new types of vibrational mode that couple particle and shape degrees of freedom. Our work provides a theoretical framework that unifies our understanding of solidification processes that take place on deformable media and lays the groundwork to exploit jamming for the control and stabilization of shape in self-assembly processes.

1 Introduction

Jamming is a transition to rigidity that occurs as bulk samples of particulate media are compressed from a freely flowing state to a solid state[1,2]. A system is jammed if it is globally rigid with respect to motions of the constituent particles. Jamming can be induced by varying thermodynamic variables such as temperature and density, as well as mechanical variables such as applied stress: Colloidal suspensions become colloidal glasses as the density is increased, flowing foams become static as the shear stress is decreased below yield stress, liquids become glasses as the temperature is lowered below the glass transition[3,4]. Moreover, in biological systems, confluent tissues also exhibit a transition to rigidity controlled by single-cell properties such as shape and motility[5–8].

In prior work, jamming has been conceived of a bulk phenomenon that takes place in a fixed geometry. There is, however, considerable recent interest in systems that involve solidification processes of particulate media embedded on deformable or moving interfaces: arrested coalescence[9] and electrically induced deformation[10] of Pickering emulsion droplets, nanoparticles driven by a moving phase boundary that form solid shells and other morphologies[11], bacteria on the interface of emulsion droplets that they gradually consume[12], and the production of jammed emulsion gels (bijels) from bicontinuous precursor mixtures[13,14]. These situations do not neatly fit into the scenarios previously envisioned, or the jamming categories proposed in prior theoretical work, because they take place on a curved and deformable surface rather than in the bulk. Here, the rigidification takes place not only with respect to particle degrees of freedom, but also with respect to the shape of the interface on which they are embedded. Further, the non-Euclidean geometry of the interface means that particles in different locations may experience location dependent states of stress depending on the local shape of the interface.

Here, we will therefore propose a new jamming class, which we refer to as *metric jamming*, that refers to structures that are rigid both with respect to particle degrees of freedom and degrees of freedom associated with the surface on which they are embedded. The purpose of this paper is to construct a model metric jamming process, explicitly test the resulting structures for rigidity and hence distinguish similarities and differences from other jammed media.

The classically jammed state is of great interest because it has unique properties compared to normal crystalline solids and new physics emerges near the jamming transition[1,4]. In contrast to crystalline solids, jammed materials generally lack translational order and are fragile, offering little or no resistance to shear deformation, and exhibit other unusual elastic properties if the particles themselves are deformable. The fragility arises from the packing's *isostaticity*, i.e. they possess only the minimal number of contacts per particle required for mechanical stability. Understanding jamming of disordered systems enables the fabrication

[a]*Department of Physics & Astronomy, Tufts University, 574 Boston Ave, Medford, MA 02155, USA.*
[b]*Electronic address: timothy.atherton@tufts.edu*

of new functional amorphous materials[15–17].

Jamming theory has been previously extended to consider non-spherical[18,19] and deformable[20,21] particles as well as to consider the role of friction[22]. In such extensions, both *hypo*static and *hyper*static configurations—those with an apparent deficit or surplus of contacts relative to the isostatic value—can emerge requiring sophisticated approaches to constraint counting[23,24] and new universality classes[25].

Two distinct theoretical approaches to jamming have been proposed: One approach considers configurations of rigid, mutually impenetrable particles under confinement[26]. Particles in a candidate structure are subjected to set of random forces ξ to find a protoypical unjamming motion δx identified by extremization of the virtual work $\xi \cdot \delta x$, a linear programming problem, subject to (linearized) interpenetrability constraints[27,28]. Analysis of the prototypical unjamming motion leads to a hierarchical classification of jammed structures[29]: A packing is *locally jammed*, the least stringent category, if no particles are able to move while the others remain fixed; it is *collectively jammed* if no subset of particles is movable with the remainder held in place; it is *strictly jammed* if no collective subset of the particles can be moved at the same time as a volume conserving deformation of the container. Our proposed metric jammed state extends this hierarchy by incorporating a flexible geometry and not simply a boundary.

An alternative approach is to consider jammed states of soft particles that interact via a short range interparticle potential $V(r)$[4]. The energy of the system is expanded as a quadratic form $U \sim \delta x \cdot H \cdot \delta x$ about a candidate jammed state of interest, where H is the Hessian matrix of the energy, also known as dynamical matrix[30–32], and δx is the displacement vector. Eigenanalysis of H is used to test the overall stability of the structure, and hence if it is truly jammed, identify particles (known as *rattlers*) that are superfluous to the rigidity. The spectrum of H also provides the density of vibrational states and therefore determines the elastic response. Jammed structures are found to possess an excess of low-frequency modes that are a signature of the fragility of the state[4,30–40]. Here, we will consider soft particles of variable rigidity, enabling us to deploy and extend the Hessian analysis to incorporate both particle and shape degrees of freedom.

2 Simulation of metric jammed structures

We consider the following scenario: suppose N soft spherical frictionless particles with different radii r_i are positioned with their centroids at coordinates $\mathbf{X}_i$ on a closed compact surface ∂C that bounds a region C of fixed volume representing, for example, an emulsion droplet. To facilitate comparisons with studies of jamming in flat space[4,36,41–46], we will use $50-50$ mixtures of bidispersed particles with radius ratio $1:1.4$ to suppress crystallization. For simplicity, we assume that the particles are rigidly confined to the surface and that their presence does not significantly deform the interface locally by forming mensici. The particles interact with one another through a potential of finite range $V(d_{ij})$ where d_{ij} is the separation of particles i and j.

The total energy of the system includes both surface tension and particle-particle interactions,

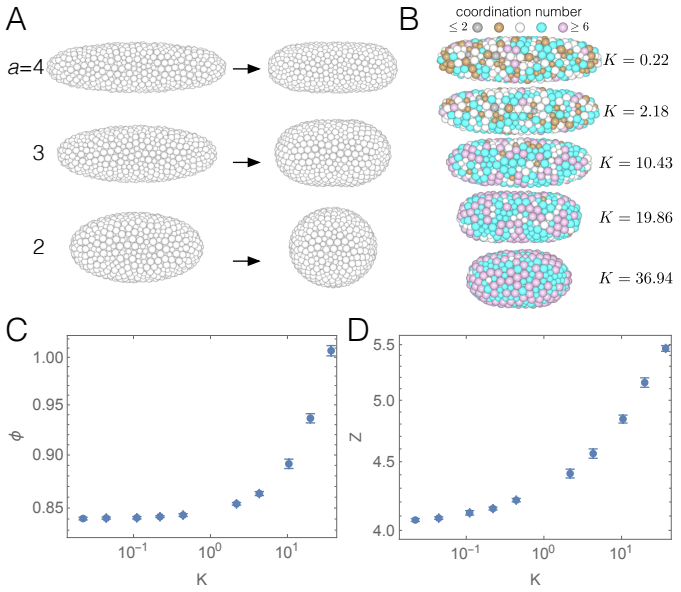

Fig. 1 Metric jammed configurations. A Initially arrested configurations on ellipsoids of varying aspect ratio (left) are relaxed into metric jammed structures (right); particles are colored by coordination number. B Metric jammed configurations as a function of $K = \sigma A/k$, a dimensionless ratio of surface and elastic energy. C Packing fraction as a function of K. D Mean contact number per particle as a function of K.

$$E = \sigma \int dA + k \sum_{i \neq j} V(d_{ij}), \tag{1}$$

where σ is the surface tension and k is the rigidity of the particles. A dimensionless ratio $K = \sigma A/k$ characterizes the relative importance of these terms where A is the surface area. The choice of surface energy here is specific to the Pickering emulsion scenario described above: The integral in (1) is over the exposed fluid-fluid interface of the emulsion droplet which might be locally deformed due to capillary effects. For simplicity, we will here assume that the particles each occupy a fixed interfacial area and instead integrate over the area of the whole surface, supplementing (1) with a constant $-\sum_i \pi r_i^2$ that does not enter into our later calculations where r_i is the radius of a single particle. Other surface energies might be applicable in different scenarios, e.g. the Helfrich energy for jamming on a vesicle[47], for example, or an elastic energy for a membrane.

The surface is parameterized by a map $\mathbf{X}(\mathbf{x}) = \mathbf{x}R(\mathbf{x})$ from points $\mathbf{x}$ that lie on the unit sphere to 3D Euclidean space where the radial function $R(\mathbf{x})$ is decomposed into tesseral harmonics,

$$R(c_{lm}, \mathbf{x}) = \sum_{lm} c_{lm} Z_{lm}(\mathbf{x}). \tag{2}$$

The configuration of the system may be fully specified by the set of parameters $\xi = \{\mathbf{x}_i, c_{lm}\}$ including N particle positions $\mathbf{x}_i$ on the unit sphere and M surface coefficients c_{lm} for a total of $2N+M$ degrees of freedom. Fixing the volume enclosed by the surface imposes a nonlinear constraint on the surface coefficients $\{c_{lm}\}$ and removes one degree of freedom. The physical position $\mathbf{X}_i$ of the ith particle may be calculated from the map $\mathbf{X}$ and depends

on $\mathbf{x}_i$ and $\{c_{lm}\}$.

For particle-particle interactions we use a compact repulsive pairwise potential[4,31,32,35,41–46,48,49],

$$V(d_{ij}) = \frac{1}{2}\left(1-\frac{d_{ij}}{s_{ij}}\right)^2 \Theta\left(\frac{d_{ij}}{s_{ij}}-1\right), \quad (3)$$

where the separation $d_{ij} = \|\mathbf{X}_i - \mathbf{X}_j\|$, $s_{ij} = r_i + r_j$ and Θ is the Heaviside step function enforcing interaction only for overlapping particles.

We construct metric jammed configurations by the following procedure: we first create rigid packings on surfaces of fixed shape, specifically ellipsoids of varying aspect ratio. These will be used to help distinguish the physical consequences of the curved geometry from those associated with the surface modes. Using the ellipsoidal packings as a starting point, we then minimize the total energy (1) of the configuration with respect to both particle and surface parameters ξ, producing a metric jammed structure. Further details are provided in the Methods section below. Fig. 1A displays initial and final states for several different aspect ratios.

For each configuration, the stability is assessed by calculating and diagonalizing the bordered Hessian of the energy functional (1) with respect to the parameter set ξ incorporating both particle and surface degrees of freedom and including the volume constraint. Particle coordinates are parametrized in spherical polar form $\mathbf{x}_i = R(\sin\theta_i\cos\phi_i, \sin\theta_i\sin\phi_i, \cos\theta_i)$. Rattlers, particles that do not contribute to the rigidity of the structure, are identified from zero modes of the Hessian associated with eigenvectors that are localized to a single particle; these particles are then removed from the structure. There also exist zero modes associated with residual degrees of freedom; for ellipsoids there is one such mode associated with cylindrical symmetry about the long axis; for spherical packings there are three. In practice, the zero modes arising from numerical calculations mix combinations of rattler and trivial motions which must be separated by Gram-Schmidt orthogonalization of the associated eigenvectors.

3 Computational Methods

Jammed configurations on fixed surfaces

We adapt the protocol for the generation of jammed configurations in 2D and 3D space[4] to packings on curved surface using the interparticle potential shown in Eq. (3). The simulation starts by randomly placing N particles of potentially different radii r_i with their centroids fixed on a curved surface that is scaled such that the area $A \gg N\pi r^2$ and hence the packing fraction $\phi \ll 1$. The simulation proceeds by iteratively reducing the size of the surface at fixed shape to slowly increase the packing fraction. Conjugate gradient descent is applied at each iteration to bring the particle interaction energy to the minimum; the sequence is terminated if the total potential energy per particle $V/N < 10^{-16}$ or V/N for successive iterations deviates by less than 10^{-15}. As the size of the surface decreases and the particles move closer to each other, inevitable overlaps appear and increase the energy minimum. The algorithm is halted if the minimized total potential energy per particle falls into $10^{-16} < V/N < 2\times10^{-16}$. This procedure brings the system extremely close to temperature $T = 0$, with a very small pressure $p < 10^{-10}$ as calculated below. These thresholds give a clear separation between jammed and unjammed state[43] and a similar approach has been utilized in other research about packings[41,42,48,50,51]. Packings are explicitly tested for rigidity by eigenanalysis as described in the main text.

Production of metric jammed configurations

We begin with a jammed packing on a fixed surface produces as described in the preceding section. Given such a configuration, described by parameters ξ, generalized forces are evaluated by taking the gradient of the energy functional (1), including the surface energy, with respect to the surface coefficients $\mathbf{f}_{c_{lm}} = -\nabla_{c_{lm}}E$. The surface is deformed along the descent direction with volume conservation by a stepsize δ and then the conjugate gradient method is employed to bring the particle system back to an energy minimum, as discussed above. The deformation is accepted if the total energy of the system afterwards is reduced, otherwise the deformation is rejected and the stepsize reduced $\delta \to \delta/2$. Further surface deformation steps are taken and the algorithm is stopped if $\delta < 10^{-16}$ or energy E for successive iterations deviates by less than 10^{-12}.

Calculation of mechanical properties

We calculate the stress tensor at each particle by constructing a local frame with tangent vectors $\mathbf{t}_\theta$ and $\mathbf{t}_\phi$ aligned in the polar and azimuthal directions respectively. The stress tensor in 2D[4,45,46,51–53] is then written as,

$$\Sigma_{\alpha\beta} = \frac{1}{A}\sum_{i>j}(r_{ij\alpha}f_{ij\beta} + r_{ji\alpha}f_{ji\beta})/2, \quad (4)$$

where A is the surface energy and $r_{ij\alpha}$, $f_{ij\beta}$ represent the projections of center-to-center distance and force along surface tangent vectors $\mathbf{t}_\theta$ and $\mathbf{t}_\phi$. The average is computed over pairs of particles. From this, we can compute the pressure $p = (\Sigma_{\theta\theta} + \Sigma_{\psi\psi})/2$, bulk modulus $B = \psi dp/d\psi$ after slightly compressing the system at packing fraction ϕ and shear modulus $G = -d\Sigma_{\theta\psi}/d\gamma$ after applying a small shear strain γ[4,45]. These variables are measured in units of k/r^2 where r is the radius of the larger particle. The shear is applied by twisting the configuration around the ellipsoid symmetry axis,

$$\psi_i = \begin{cases} \psi_i + 2\theta_i\gamma & 0 \le \theta_i < \pi/2 \\ \psi_i + 2(\theta_i - \pi)\gamma & \pi/2 < \theta_i \le \pi \end{cases}. \quad (5)$$

after which we apply the conjugate gradient descent method to minimize the energy while fixing the position of several particles near the poles; these fixed particles and the area they cover are excluded from the stress tensor calculation.

4 Results

Metric jammed structures range from iso- to hyperstatic

Metric jammed structures for different values of K are shown in Fig. 1B with the local coordination number indicated. For large K, where the surface tension is large, the final shape tends to-

wards spherical, and hence achieves a globally minimal surface; particles tend to higher coordination numbers. For smaller K, or larger inter-particle interaction energies, the shape instead tends toward spherocylindrical and the average coordination number tends to 4. Inspecting the spatially resolved distribution of coordination numbers along the structure, we do not see significant variation. This is in contrast to the situation with monodisperse particles on a fixed surface where variations in the distribution of defects can be predicted from the curvature[54], but could be due to the limited size of our dataset.

From the structures we can compute two structural measures, an estimate of the packing fraction,

$$\phi = \left(N\pi \sum_i r_i^2 \right) / A. \tag{6}$$

where A is the area of the surface at the jamming point, and the mean number of contacts per particle Z. Both ϕ and Z are signatures of jamming in flat space. Fig. 1C displays ϕ as a function of K: As $K \to 0$, ϕ approaches the value of 0.84 characteristic of random close packing in 2D space[4,55]. Note that because the particles remain confined to the surface, and are not packed in three dimensions, the two dimensional value is to be expected. As K increases further, the particles are increasingly compressed and the exposed surface gradually eliminated. Because our estimate of ϕ in Eq. (6) does not account for overlap between particles, the value of ϕ exceeds 1 for sufficiently large K; the true packing fraction tends $\phi \to 1$ for large K. We use this simple estimate here because we are primarily interested in the behavior near the jamming point, and a more careful calculation requires us to project the particles onto the surface accounting for the local curvature.

The mean contact number Z is plotted with respect to K in Fig. 1D and tends towards 4 as $K \to 0$ which for $K \to 10$ the number of contacts is significantly greater, reaching values as high as 5.5.

We now compare these results with the situation in flat space. A linear constraint counting argument due to Maxwell[56] and developed by Calladine[57,58] predicts the minimal number of contacts: the number of degrees of freedom for N particles is dN where d is the dimensionality and ξ is the number of residual degrees of freedom in the space ($\xi = d$ in d-dimensional space and $\xi = 1$ for cylindrically symmetric surfaces as discussed above). These must be balanced by $NZ_{iso}/2$ constraints, i.e. $dN = NZ_{iso}/2 + \xi$. The isostatic contact number in 2D is therefore $Z_{iso} = 4 - 4/N$. Previous literature demonstrates that an additional degree of freedom is required to maintain positive pressure and bulk modulus in flat space, such that $dN + 1 = NZ_c + \xi$ [44,59].

The contact number at jamming is $Z_c = 4 - 2/N$ on 2D flat surfaces and $Z_c = 4$ on cylindrically symmetric surfaces. Hence, the metric jammed structures displayed in Fig. 1 appear *hyperstatic* relative to the Maxwell value and tend towards the isostaticity observed in flat space only as $K \ll 1$, i.e. where the rigidity of the particles is significantly greater than the surface tension. In that limit, the packing fraction approaches the random close packing value.

The Maxwell argument does not, however, account for the curvature of the surface on which the particles are embedded, or

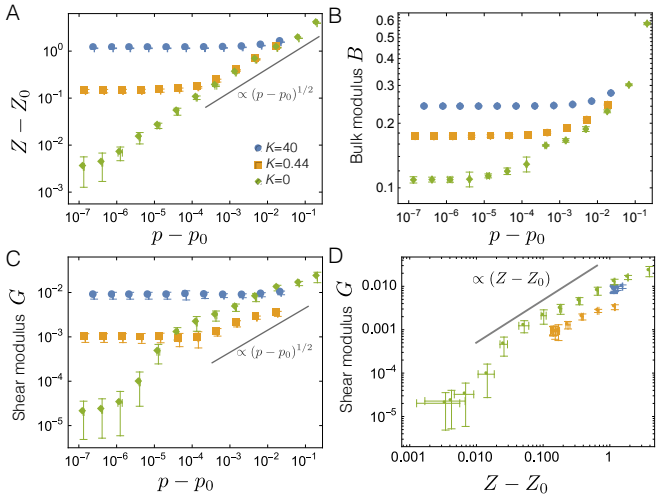

Fig. 2 Mechanical properties of metric jammed configurations. A change in contact number as a function of pressure. Elastic moduli as a function of pressure for different K: B bulk modulus and C shear modulus. D The shear modulus is also shown versus contact number.

stresses induced by the surface tension term. Recent work on granular media in flat space but with internal stresses has shown that under compression the system becomes rigid at contact numbers larger than the Maxwell value[60], which could explain the abundance of large contact values at large K. More generally, criteria for rigidity remain a problem of interest beyond jamming. Some have attempted to incorporate energetic arguments into the Maxwell argument[61]; others have proposed alternative criteria based on energetic rigidity[62].

Shear modulus strongly depends on particle rigidity

Jammed structures in 2D flat space also exhibit a unique elastic response: they possess vanishing shear modulus, and exhibit characteristic scalings of the pressure $p \sim (\phi - \phi_0)^1$, excess contact number $\Delta Z \equiv Z - Z_{iso} \sim (\phi - \phi_0)^{1/2}$, bulk and shear elastic moduli $B \sim (\phi - \phi_0)^0$, $G \sim (\phi - \phi_0)^{1/2}$ as the system is compressed beyond the jamming point ϕ_0 [2,4,44,59,63]. To test this, we deform metric jammed configurations in two ways: the structure is compressed slightly to measure the bulk modulus B and a twist deformation is imposed about the symmetry axis to measure the shear modulus G. The elastic moduli are computed from derivatives of the stress tensor during the deformation as described in Methods and results for packings with different K are displayed in Fig. 2.

We established that the excess pressure $\Delta p = p - p_0$ is linearly proportional to the excess packing fraction $\phi - \phi_0$ and is therefore a good measure of the deformed system's proximity to the jamming point. The excess contact number, bulk modulus and shear modulus are therefore displayed as a function of Δp in Fig. 2(a)-(c). The excess coordination number displays an initial plateau but then increases at a critical pressure that increases with K. Far from the jamming point, we find that the excess contact number scales as $\Delta Z \sim (\Delta p)^{0.5}$. The bulk modulus possesses a similar plateau for all K at low Δp.

The shear modulus G is several orders of magnitude smaller

than the bulk modulus, and strongly depends on the value of K. For large K, G is finite and constant as $\Delta p \to 0$ and scales approximately like $(\Delta p)^{0.5}$ at larger Δp. For small K the trend is more complex, tending to zero at small Δp but exhibiting a shoulder. To understand this in more detail, we plot G as a function of the excess contact number ΔZ in Fig. 2(d). As discussed in[37], if G scales like ΔZ then the elasticity is nonaffine, while if $G \propto Z$ the elasticity is affine. While the trend at low K is complicated, the results are more consistent with non-affine elasticity. In[54] we saw significant evidence of non-affine deformation in the kinetics of particulate media on a bisphere, and hence it is quite possible we might be able to resolve these effects in future work.

Overall, these results reproduce the behavior of jammed packings in flat space at low K reasonably well. As $K \gg 1$, the structures begin to resemble normal solids where $G \sim (\phi - \phi_c)^0$ [2,4,44,59] even though G remains small.

Vibrational analysis reveals new mode types

A third signature of the jammed state is an excess of low frequency vibrational modes[4,30–32,34–36,38,40,64–66], in contrast to the Debye theory of elastic solids[67,68]. Eigenanalysis of the Hessian matrix provides the vibrational frequencies, which are the square roots of the eigenvalues measured in units of $\sqrt{k}/r$ where r is the radius of the larger particle, and associated vibrational modes from the eigenvectors. We display the density of states $D(\omega)$ for different values of K in Fig. 3A at several values of $\Delta\phi = \phi - \phi_0$. Two key features are apparent: first, $D(\omega)$ possesses a low frequency plateau characteristic of jamming for low K and at low $\Delta\phi$. As the system is compressed, or as K increases, the plateau vanishes leading to Debye-like behavior.

A second feature is that $D(\omega)$ falls abruptly above a critical value of ω. The transition is very sharp as $K \to 0$ and smoothed out for larger K. In Fig. 3B, we display the component of the eigenvectors in the polar direction as a function of ω, close to the metric jammed configuration. At low frequency, particles tend to vibrate along the azimuthal ϕ direction while high-frequency localized vibrations are along the polar θ direction. The crossover of $D(\omega)$ coincides with the transition of particle motions. For packings on spherical surfaces the high frequencies have motions both along θ and ϕ directions due to the symmetric nature. Hence spatially inhomogeneous curvature can cause the localization of vibrational modes.

The participation ratio $P(\omega)$ is calculated to characterize the vibrational modes[32,34,40,48,65]. It is a measure of the fraction of particles that are participating in the motion governed by the mode of frequency ω. Given the eigenvectors $\{\vec{u}_i(\omega)\}$ at frequency ω for every particle,

$$P(\omega) = \frac{1}{N} \frac{(\sum_i \|u_i(\omega)\|^2)^2}{\sum_i \|u_i(\omega)\|^4}, \tag{7}$$

where N is the number of particles after removing ratters. On the curved surfaces considered here, we use the arclength to represent $\|u_i(\omega)\|^2$.

The corresponding participation ratios $P(\omega)$ are also displayed in Fig. 3C together with illustrations of typical vibrational modes in Fig. 3D for configurations close to the metric jamming point with $K = 40$, revealing the consequences of anisotropic curvature. In the low-frequency region far from the jamming point, plane-wave like phonon modes (Fig. 3D ii) and quasi-localized modes (Fig. 3D iii) where localized excitations are visible on a small plane-wave background. In the mid-frequency region, we have extended modes where random excitations spread throughout the entire system along the azimuthal ϕ direction (Fig. 3D iv), and along the polar θ direction (Fig. 3D v) for larger frequencies. The high-frequency region contains localized modes where only a few particles vibrate along the polar θ direction(Fig. 3D vi). These vibrational modes also exists for jammed structures on flat surfaces[1,2,36,40,65,69]. The spatially inhomogeneous curvature, however, causes the extended modes along the polar θ or azimuthal ϕ direction. Additionally for metric jammed configurations at very low frequency where the component of eigenvectors along θ direction and participation ratio are almost 1, there appears a vibrational mode where all particles move along the θ direction, showed in Fig. 3i.

Our inclusion of shape as well as particulate degrees of freedom allows for the possibility of new modes with mixed character. To examine this, we display in Fig. 4A and B the projection of each normalized eigenvector that lies in the shape sector, $c(\omega)$, as a function of the angular frequency. We see that modes associate with significant shape deformation tend to lie in the high frequency regime, relatively independently of K. Two such modes are depicted in Fig. 4C and D.

5 Conclusion

These results collectively show that particulate media on deformable surfaces can form structures that share structural and mechanical properties with conventional jammed media in Euclidean space, but are rigid with respect to surface as well as particle degrees of freedom. Experimentally produced structures are likely to initially be arrested, i.e. only locally jammed, but by successive unjamming and relaxation events proceed toward a new *metric jammed* state that is rigid with respect to surface as well as particle degrees of freedom. The presence of a surface energy tends to compress the particles somewhat in the metric jammed state, and hence metric jammed structures resemble those in flat space only in the limit of high particle rigidity. By adjusting the relative influence of surface and particle energies characterized by a single dimensionless parameter $K = \sigma A/k$, metric jammed structures can continuously be tuned from isostatic with vanishing shear modulus, i.e. similar to jammed states in flat space, to states that resemble conventional elastic solids. A simple structural metric, the coordination number, serves as an indicator of where in this range a particular candidate structure lies. The vibrational spectrum may similarly be tuned from similar to a jammed solid, possessing an excess of low frequency modes, to Debye-like. In either case, the curved space leaves a significant imprint on the spectrum, leading to localized and oriented modes due to the anisotropic curvature.

Our work provides a theoretical framework that unifies our understanding of solidification processes that take place on deformable media and extends the applicability of the jamming con-

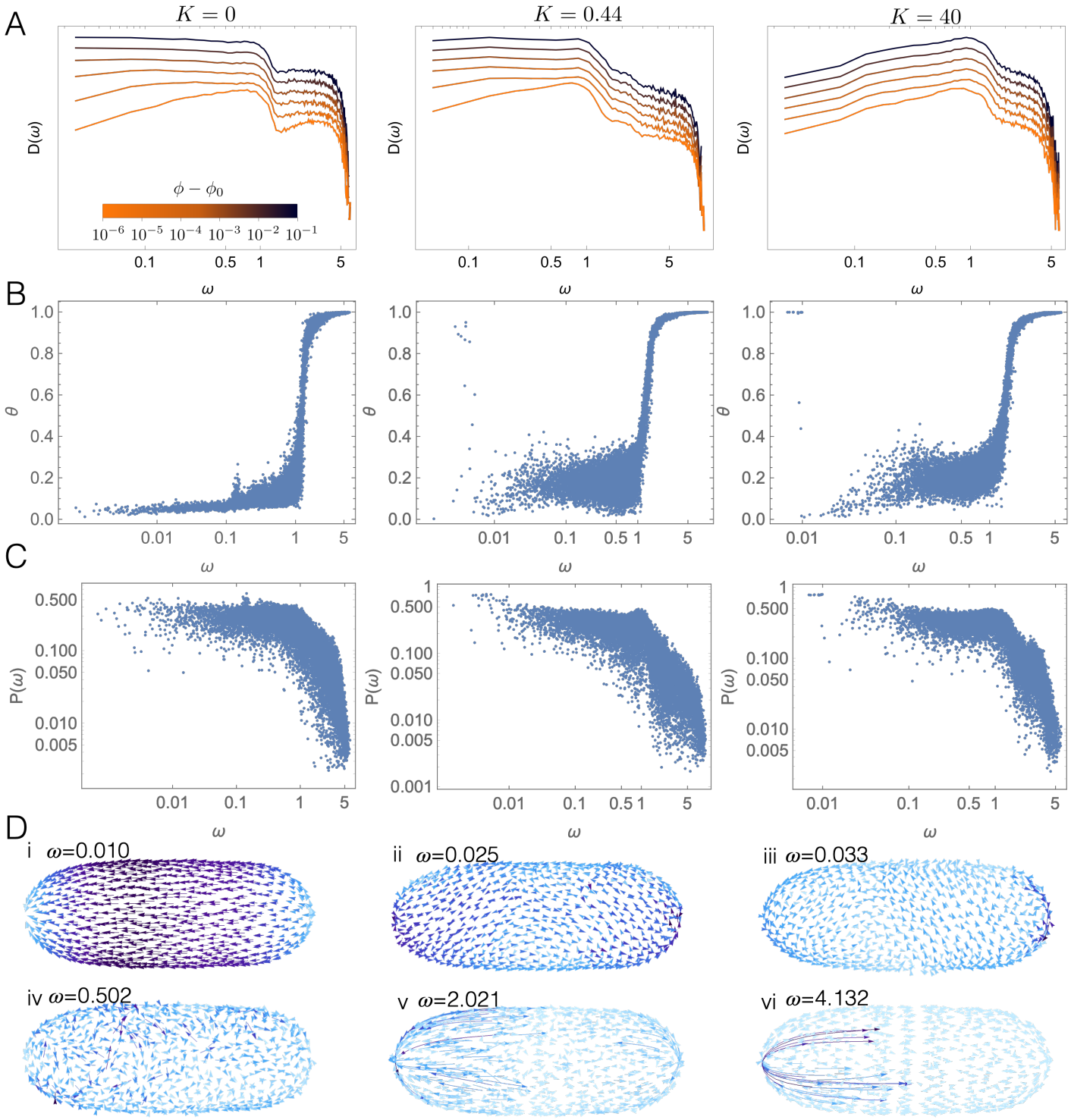

Fig. 3 Vibrational properties of metric jammed configurations. A Vibrational density of states $D(\omega)$, B vibrational component along polar axis for $\phi - \phi_0 = 10^{-6}$ and C participation ratio $P(\omega)$ for metric jammed configuraion with $K = 0$, $K = 0.44$ and $K = 40$ at $\phi - \phi_0 = 10^{-6}$. D Selected vibrational modes for $K = 40$: i translation along polar direction, ii phonon mode, iii quasi-localized mode, iv extended mode along polar direction, v extended mode along azimuthal direction, vi localized mode.

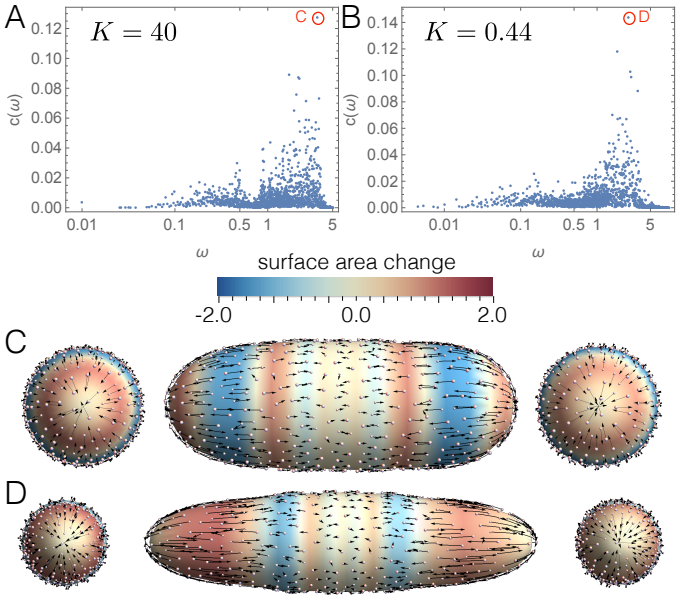

Fig. 4 Combined shape-particle vibrational modes. A Projection $c(\omega)$ of the eigenvector associated with the shape deformation sector for rigid particles $K = 40$ and B $K = 0.44$. C and D Representative eigenvectors with significant shape and particle deformation; the local rate of change in area is plotted together with arrows indicating particle motions.

cept. In the Pickering emulsion platform considered here, particles are used to control the stability and, ultimately, the droplet size as metric jamming protects droplets from coalescence[9]. In these materials, a deeper understanding of the mechanisms underpinning stability could facilitate sculpting of new shapes beyond those already demonstrated using micromanipulation, flow or coalescence[70]. Applications of Pickering emulsions abound in food science[71], biomimetic synthesis[72] and inkjet printing of morphology[73] which could all benefit from such understanding.

Beyond emulsions, the results may provide fresh insight into other materials such as bijels[13,14] that rely on such processes. A particularly exciting potential class of applications lies in biological matter, given the remarkable success in applying ideas from jamming to tissues and particularly tumor progression[5–8].

Future work should aim to integrate other developments from the jamming community, such as nonspherical particles and deformability[7,18,20,25], to elucidate possible connections between the shape of the confining surface and particle shape. Even in the absence of curvature, these complicates the jamming scenario: ellipsoidal particles, for example, pack at higher densities and introduce rotational degrees of freedom[74,75]. Nonspherical deformable particles exhibit very different vibrational properties depending on whether they cost energy to bend[21]. In the metric jamming scenario, these effects could depend on the local curvature and be influenced by the shape degrees of freedom. Here we have restricted our attention solely to convex geometries but non-convex morphologies could also be readily created; these must necessarily include regions of negative gaussian curvature that tend to promote higher local coordination number. In previous work on the arrest of bispherical droplets, we showed that such regions tended to localize defects and were responsible for kinetic effects on the local order[54].

While the configurations observed here appeared to be hyperstatic, the nontrivial coupling of surface and particle degrees of freedom, and the new kinds of deformation mode that can emerge, connect with the recently identified need for more sophisticated approaches to characterizing rigidity[62]. The presence of curvature causes different parts of a metric jammed structure to be under different degrees of compression, which may lead to variation in the local criterion for isostaticity[60]. A much larger numerical study of a suitable ensemble of structures should be performed to resolve this and other spatial variations in ordering, including non-affine deformations[37]. Generalizing our approach to more complicated geometries, including those that are non-convex as we did in[54] is also of considerable interest. Additionally, alternative representations of parameterizations of the shape should be studied with more degrees of freedom included; we are presently working on generalizing our results to jamming on simplicial complexes for example.

Experimentally, the interplay of order and shape that emerges in metric jamming suggests the possibility of assembly processes that sculpt particulate media into a desired configuration by exploiting deformable interfaces; our framework provides a unified understanding to facilitate their design.

Conflicts of interest

There are no conflicts to declare.

Acknowledgements

We thank P. Spicer and A. Donev for helpful discussions. This material is based upon work supported by the National Science Foundation under Grant No. DMR-1654283.

Notes and references

1 M. van Hecke, *Journal of Physics: Condensed Matter*, 2009, **22**, 033101.
2 A. J. Liu and S. R. Nagel, *Annu. Rev. Condens. Matter Phys.*, 2010, **1**, 347–369.
3 A. J. Liu and S. R. Nagel, *Nature*, 1998, **396**, 21–22.
4 C. S. O'hern, L. E. Silbert, A. J. Liu and S. R. Nagel, *Physical Review E*, 2003, **68**, 011306.
5 D. Bi, J. Lopez, J. M. Schwarz and M. L. Manning, *Nature Physic*, 2015, **11**, 1074–1079.
6 D. Bi, X. Yang, M. C. Marchetti and M. L. Manning, *Physical Review X*, 2016, **6**, 021011.
7 S. Grosser, J. Lippoldt, L. Oswald, M. Merkel, D. M. Sussman, F. Renner, P. Gottheil, E. W. Morawetz, T. Fuhs, X. Xie *et al.*, *Physical Review X*, 2021, **11**, 011033.
8 L. Oswald, S. Grosser, D. M. Smith and J. A. Käs, *Journal of physics D: Applied physics*, 2017, **50**, 483001.
9 A. B. Pawar, M. Caggioni, R. Ergun, R. W. Hartel and P. T. Spicer, *Soft Matter*, 2011, **7**, 7710–7716.
10 A. Mikkelsen and Z. Rozynek, *ACS applied materials & interfaces*, 2019, **11**, 29396–29407.

11 A. L. Rodarte, R. J. Pandolfi, S. Ghosh and L. S. Hirst, *Journal of Materials Chemistry C*, 2013, **1**, 5527 – 7.

12 L. S. Dorobantu, A. K. Yeung, J. M. Foght and M. R. Gray, *Applied and environmental microbiology*, 2004, **70**, 6333–6336.

13 K. Stratford, R. Adhikari, I. Pagonabarraga, J.-C. Desplat and M. E. Cates, *Science*, 2005, **309**, 2198–2201.

14 E. M. Herzig, K. A. White, A. B. Schofield, W. C. Poon and P. S. Clegg, *Nature materials*, 2007, **6**, 966–971.

15 J. R. Stokes and W. J. Frith, *Soft Matter*, 2008, **4**, 1133–1140.

16 J. Mattsson, H. M. Wyss, A. Fernandez-Nieves, K. Miyazaki, Z. Hu, D. R. Reichman and D. A. Weitz, *Nature*, 2009, **462**, 83–86.

17 D. Vlassopoulos and M. Cloitre, *Current opinion in colloid & interface science*, 2014, **19**, 561–574.

18 K. VanderWerf, W. Jin, M. D. Shattuck and C. S. OHern, *Physical Review E*, 2018, **97**, 012909.

19 Y. Yuan, K. VanderWerf, M. D. Shattuck and C. S. OHern, *Soft matter*, 2019, **15**, 9751–9761.

20 J. D. Treado, D. Wang, A. Boromand, M. P. Murrell, M. D. Shattuck and C. S. O'Hern, *Physical Review Materials*, 2021, **5**, 055605.

21 D. Wang, J. D. Treado, A. Boromand, B. Norwick, M. P. Murrell, M. D. Shattuck and C. S. O'Hern, *Soft Matter*, 2021, **17**, 9901–9915.

22 D. Bi, J. Zhang, B. Chakraborty and R. P. Behringer, *Nature*, 2011, **480**, 355–358.

23 S. Henkes, D. A. Quint, Y. Fily and J. M. Schwarz, *Physical review letters*, 2016, **116**, 028301.

24 S. Papanikolaou, C. S. OHern and M. D. Shattuck, *Physical review letters*, 2013, **110**, 198002.

25 C. Brito, H. Ikeda, P. Urbani, M. Wyart and F. Zamponi, *Proceedings of the National Academy of Sciences*, 2018, **115**, 11736–11741.

26 S. Torquato and F. H. Stillinger, *Reviews of modern physics*, 2010, **82**, 2633.

27 A. Donev, S. Torquato, F. H. Stillinger and R. Connelly, *Journal of applied physics*, 2004, **95**, 989–999.

28 A. Donev, S. Torquato, F. H. Stillinger and R. Connelly, *Journal of Computational Physics*, 2004, **197**, 139–166.

29 S. Torquato and F. H. Stillinger, *The Journal of Physical Chemistry B*, 2001, **105**, 11849–11853.

30 M. Wyart, S. R. Nagel and T. A. Witten, *EPL (Europhysics Letters)*, 2005, **72**, 486.

31 M. Wyart, L. E. Silbert, S. R. Nagel and T. A. Witten, *Physical Review E*, 2005, **72**, 051306.

32 P. Charbonneau, E. I. Corwin, G. Parisi, A. Poncet and F. Zamponi, *Physical review letters*, 2016, **117**, 045503.

33 A. Ghosh, V. K. Chikkadi, P. Schall, J. Kurchan and D. Bonn, *Physical review letters*, 2010, **104**, 248305.

34 K. Chen, W. G. Ellenbroek, Z. Zhang, D. T. Chen, P. J. Yunker, S. Henkes, C. Brito, O. Dauchot, W. Van Saarloos, A. J. Liu *et al.*, *Physical review letters*, 2010, **105**, 025501.

35 L. E. Silbert, A. J. Liu and S. R. Nagel, *Physical review letters*, 2005, **95**, 098301.

36 L. E. Silbert, A. J. Liu and S. R. Nagel, *Physical Review E*, 2009, **79**, 021308.

37 A. Zaccone and E. Scossa-Romano, *Phys. Rev. B*, 2011, **83**, 184205.

38 E. DeGiuli, A. Laversanne-Finot, G. Düring, E. Lerner and M. Wyart, *Soft Matter*, 2014, **10**, 5628–5644.

39 M. L. Manning and A. J. Liu, *EPL (Europhysics Letters)*, 2015, **109**, 36002.

40 F. Arceri and E. I. Corwin, *Physical Review Letters*, 2020, **124**, 238002.

41 G.-J. Gao, J. Bławzdziewicz and C. S. O'Hern, *Physical Review E*, 2006, **74**, 061304.

42 N. Xu, J. Blawzdziewicz and C. S. O'Hern, *Physical Review E*, 2005, **71**, 061306.

43 D. Vågberg, P. Olsson and S. Teitel, *Physical Review E*, 2011, **83**, 031307.

44 C. P. Goodrich, A. J. Liu and S. R. Nagel, *Physical review letters*, 2012, **109**, 095704.

45 S. Chen, T. Bertrand, W. Jin, M. D. Shattuck and C. S. O'Hern, *Physical Review E*, 2018, **98**, 042906.

46 A. Boromand, A. Signoriello, J. Lowensohn, C. S. Orellana, E. R. Weeks, F. Ye, M. D. Shattuck and C. S. O'Hern, *Soft matter*, 2019, **15**, 5854–5865.

47 W. Helfrich, *Zeitschrift für Naturforschung C*, 1973, **28**, 693–703.

48 N. Xu, V. Vitelli, A. J. Liu and S. R. Nagel, *EPL (Europhysics Letters)*, 2010, **90**, 56001.

49 K. VanderWerf, A. Boromand, M. D. Shattuck and C. S. O'Hern, *Physical Review Letters*, 2020, **124**, 038004.

50 M. Mailman, C. F. Schreck, C. S. O'Hern and B. Chakraborty, *Physical review letters*, 2009, **102**, 255501.

51 C. F. Schreck, N. Xu and C. S. O'Hern, *Soft Matter*, 2010, **6**, 2960–2969.

52 M. P. Allen and D. J. Tildesley, *Computer simulation of liquids*, Oxford university press, 2017.

53 C. P. Goodrich, A. J. Liu and J. Sethna, *Proceedings of the National Academy of Sciences*, 2016, **113**, 9745–9750.

54 Z. Xie, C. J. Burke, B. Mbanga, P. T. Spicer and T. J. Atherton, *Soft Matter*, 2019, **15**, 9587–9596.

55 A. Zaccone, *Physical Review Letters*, 2022, **128**, 028002.

56 J. C. Maxwell, *The London, Edinburgh, and Dublin Philosophical Magazine and Journal of Science*, 1864, **27**, 294–299.

57 C. R. Calladine, *International journal of solids and structures*, 1978, **14**, 161–172.

58 T. Lubensky, C. Kane, X. Mao, A. Souslov and K. Sun, *Reports on Progress in Physics*, 2015, **78**, 073901.

59 C. P. Goodrich, S. Dagois-Bohy, B. P. Tighe, M. van Hecke, A. J. Liu and S. R. Nagel, *Physical Review E*, 2014, **90**, 022138.

60 B. Cui, G. Ruocco and A. Zaccone, *Granular Matter*, 2019, **21**, 1–6.

61 J. W. Rocks and P. Mehta, *arXiv preprint arXiv:2208.07419*, 2022.

62 O. K. Damavandi, V. F. Hagh, C. D. Santangelo and M. L. Man-

ning, *arXiv preprint arXiv:2102.11310*, 2021.
63 M. Schlegel, J. Brujic, E. Terentjev and A. Zaccone, *Scientific reports*, 2016, **6**, 1–8.
64 R. Milkus and A. Zaccone, *Phys. Rev. B*, 2016, **93**, 094204.
65 H. Mizuno, H. Shiba and A. Ikeda, *Proceedings of the National Academy of Sciences*, 2017, **114**, E9767–E9774.
66 L. Wang, A. Ninarello, P. Guan, L. Berthier, G. Szamel and E. Flenner, *Nature communications*, 2019, **10**, 1–7.
67 P. Debye, *Annalen der Physik*, 1912, **344**, 789–839.
68 R. Zeller and R. Pohl, *Physical Review B*, 1971, **4**, 2029.
69 Z. Zeravcic, W. van Saarloos and D. R. Nelson, *EPL (Europhysics Letters)*, 2008, **83**, 44001.
70 M. Cui, T. Emrick and T. P. Russell, *Science*, 2013, **342**, 460–463.
71 C. C. Berton-Carabin and K. Schroën, *Annual review of food science and technology*, 2015, **6**, 263–297.
72 M. Zhang, R. Ettelaie, L. Dong, X. Li, T. Li, X. Zhang, B. P. Binks and H. Yang, *Nature Communications*, 2022, **13**, 475.
73 J. Sun, B. Bao, M. He, H. Zhou and Y. Song, *ACS applied materials & interfaces*, 2015, **7**, 28086–28099.
74 A. Donev, F. H. Stillinger, P. Chaikin and S. Torquato, *Physical review letters*, 2004, **92**, 255506.
75 A. Donev, R. Connelly, F. H. Stillinger and S. Torquato, *Physical Review E*, 2007, **75**, 051304.